MSAS – Final project

Paola Pia Foligno (945677), Anna Fontan (945648), Alessio Gigante (953558)

1 The real system

ESA's Gravity field and Ocean Circulation Explorer (GOCE) orbited as close to Earth as possible, to maximise its sensitivity to variations in Earth's gravity field [3]. GOCE's mission had several objectives: mapping Earth's geoid, as well as estimating precisely the marine geoid, needed for the quantitative determination of absolute ocean currents and their transport of heat; this brought to a new understanding of the physics of Earth's interior. GOCE provided also a better global height reference system for datum connection, which can serve as a reference surface for the study of topographic processes, such as the evolution of ice-sheets and land surface. Ultimately, it estimated the thickness of the polar ice sheets. In order to accomplish these tasks, GOCE made use of three pairs of accelerometers to measure the gravity gradients along the three orthogonal axes. However, to have accurate measurements GOCE had to orbit really close to the Earth; hence, without an ion propulsion system that provided thrust to counteract the drag, the spacecraft would have experienced a fast orbit decay.

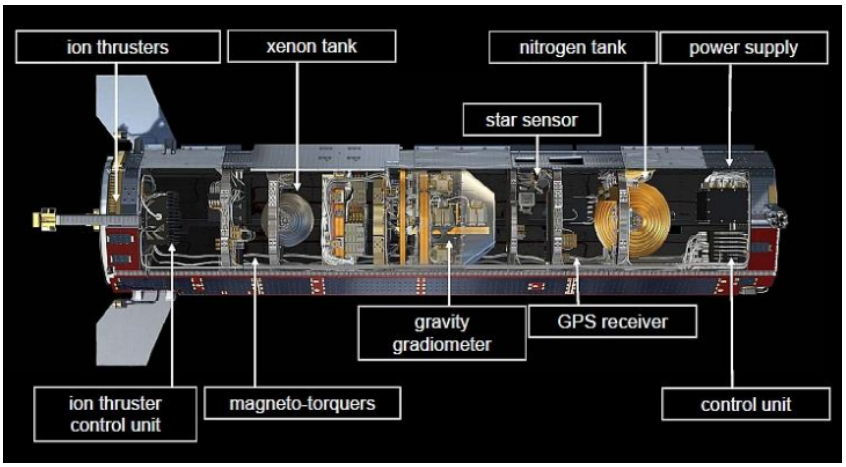

Figure 1: Scheme of GOCE spacecraft [3].

GOCE system had some key components, which granted the results obtained during its years of orbiting; they are highlighted in Fig. 1. The spacecraft started operating at an altitude of 254.9 km, on a sun-synchronous orbit [3]. During the mission, the satellite reached altitudes of about 170 km, with atmospheric drag levels at an average of over 50 mN. The spacecraft continued to perform excellently at these extreme conditions [2]. Moreover, around the end of mission the pressure in GOCE's fuel system has dropped below 2.5 bar, which is the pressure needed to fire the ion engine. Anyhow, the system kept working until it ran out of Xenon [2].

2 The physical model

The physical model consists of the following four subsystems, related to:

1. orbital mechanic: here, in order to compute the drag, a model of the atmosphere of the Earth has been considered, which is the DMT-2013 Thermosphere one [1]; in particular, it has been chosen since it is based on the measurements taken from GOCE mission [8]. Moreover, to evaluate the altitude in each point, the Earth has been modeled as a 2D ellipsoid with given semi-major axis and semi-minor axis. Indeed, this evaluation can be done assuming that GOCE operates on a polar orbit, i.e. the inclination remains practically constant with time. One of the inputs of this subsystem is the thrust;

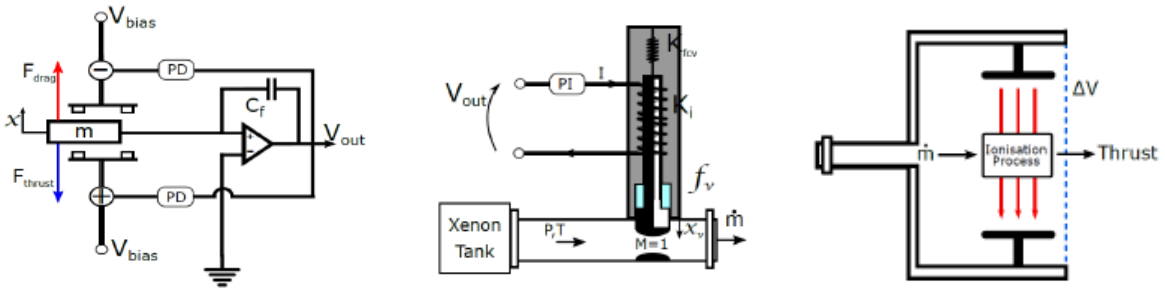

(a) gradiometer **(b)** flow control valve **(c)** ion engine

Figure 2: Physical models

2. accelerometer: here the main principle is that a proof mass floats in a small cage and is kept in the centre of it by electrostatic forces, i.e. by applying voltages between the cage and the different sides of the proof mass itself. These voltages are also representatives to the external accelerations seen by the proof mass [6]. In order to simplify the model, only one accelerometer (with the thrust as input and V_{OUT} as output) has been taken into account and its displacement is aligned with the direction of the velocity;

3. flow control valve: here the electrical, mechanical, and hydraulic domains are considered. This system (which input is the V_{OUT} and the output $\dot{m}$) is composed by a coil (ideal inductor) wrapped around a spool, which is connected to a spring (ideal); the spool, initially closed, obstructs Xenon flow in a duct which leads to the ion engine. Due to an input voltage, the current inside the coil activates the spool by means of an induced magnetic force, which will lift it up, letting the requested amount of Xenon to reach the engine. In order to simplify the model, the force applied on the spool by the fluid has been neglected, as well as the valve leakage, and the flow is approximated as one-dimensional;

4. ion thruster: the considered assembly is QinetiQ T5 ion engine and it is a gridded ion thruster with a direct current discharge between a hollow cathode and a cylindrical anode, used to ionise propellant gas. The efficiency of the plasma production process is enhanced by the application of a weak and variable magnetic field within the discharge chamber [7]. In order to simplify the mathematical model (which input is $\dot{m}$ and output the thrust), the electric field is assumed to be uniform and the flow one-dimentional; acceleration grids bring ions to a final velocity starting from v = 0; grids erosion has been neglected, as well as the thrust static contribution ($\text{P}_{\text{EXT}} = 0$) [5].

3 The mathematical model

In order to describe the mathematical model of the orbital mechanic system, initially the perturbing accelerations due to the J_2 and the drag have been defined respectively in Eq. 1 and Eq. 2 [4].

$$\mathbf{p_{J_2}} = \frac{3}{2}\frac{J_2\mu_\oplus a^2}{R^4}\left[\frac{R_x}{R}\left(5\frac{R_z^2}{R^2}-1\right), \frac{R_y}{R}\left(5\frac{R_z^2}{R^2}-1\right), \frac{R_z}{R}\left(5\frac{R_z^2}{R^2}-3\right)\right]^T \tag{1}$$

$$\mathbf{p_D} = -\frac{\rho}{2\beta}\mathbf{v}_{\text{REL}}|\mathbf{v}_{\text{REL}}| \tag{2}$$

$$\mathbf{p_T} = \frac{\mathbf{T}}{M} \tag{3}$$

where R is the norm of GOCE position vector $\mathbf{R}$. Moreover, the acceleration linked to the thrust needed to counteract the drag is reported in Eq. 3.
To obtain the Gauss Planetary Equations the three perturbing accelerations have to be considered in the LVLH (Local Vertical Local Horizontal) frame; hence, hereafter (Eqs. 4, 5 and 6) the orthogonal unit vectors of this reference frame are reported as well as the resultant components

of the perturbing accelerations in this reference frame (Eqs. 8, 9 and 10)

$$\mathbf{r} = \begin{bmatrix} -\sin\Omega\cos i\sin u + \cos\Omega\cos u \\ \cos\Omega\cos i\sin u + \sin\Omega\cos u \\ \sin i\sin u \end{bmatrix} \quad (4) \qquad \mathbf{s} = \begin{bmatrix} -\sin\Omega\cos i\cos u - \cos\Omega\sin u \\ \cos\Omega\cos i\cos u - \sin\Omega\sin u \\ \sin i\cos u \end{bmatrix} \quad (5)$$

$$\mathbf{w} = \begin{bmatrix} \sin\Omega\sin i \\ -\cos\Omega\sin i \\ \cos i \end{bmatrix} \quad (6)$$

where the parameter u, i.e. the argument of latitude, is given by Eq. 7.

$$u = \theta + \omega \quad (7) \qquad p_{\mathrm{R}} = (\mathbf{p_{J_2}} + \mathbf{p_D} + \mathbf{p_T}) \cdot \mathbf{r} \quad (8)$$

$$p_{\mathrm{S}} = (\mathbf{p_{J_2}} + \mathbf{p_D} + \mathbf{p_T}) \cdot \mathbf{s} \quad (9) \qquad p_{\mathrm{W}} = (\mathbf{p_{J_2}} + \mathbf{p_D} + \mathbf{p_T}) \cdot \mathbf{w} \quad (10)$$

Therefore, the Gauss Planetary Equations are given by Eqs. 11 to 16:

$$\begin{cases} \dot{h} = R\,p_{\mathrm{S}} & (11) \\ \dot{e} = \dfrac{h}{\mu_\oplus}\sin\theta\,p_{\mathrm{R}} + \dfrac{p_{\mathrm{S}}}{\mu_\oplus h}\left[(h^2 + \mu_\oplus R)\cos\theta + \mu_\oplus R\,e\right] & (12) \\ \dot{i} = \dfrac{R}{h}\cos u p_{\mathrm{W}} & (13) \\ \dot{\Omega} = \dfrac{R\sin u}{h\sin i}p_{\mathrm{W}} & (14) \\ \dot{\omega} = -\dfrac{1}{eh}\left[\dfrac{h^2}{\mu_\oplus}\cos\theta\,p_{\mathrm{R}} - \left(R + \dfrac{h^2}{\mu_\oplus}\sin\theta\,p_{\mathrm{S}}\right)\right] - \dfrac{R\sin u}{h\tan i}p_{\mathrm{W}} & (15) \\ \dot{\theta} = \dfrac{h}{R^2} + \dfrac{1}{eh}\left[\dfrac{h^2}{\mu_\oplus}\cos\theta\,p_{\mathrm{R}} - \left(\dfrac{h^2}{\mu_\oplus} + R\right)\sin\theta\,p_{\mathrm{S}}\right] & (16) \end{cases}$$

The accelerometer instead consists of parallel plates, which capacitances between the rotor and the first and second stators are defined respectively in Eqs. 17 and 18.

$$C_1 = \frac{\epsilon A}{g - x_{\mathrm{A}}} \quad (17) \qquad C_2 = \frac{\epsilon A}{g + x_{\mathrm{A}}} \quad (18)$$

If the rotor, hence the mass, is assumed in its middle position then no signal can be provided to the OPAMP and only the external loop (in Fig. 2a) is taken into account.
Furthermore, considering the equivalent capacitance too (see Eq. 19), the current across the capacitors can be evaluated as shown in Eq. 20.

$$C_{\mathrm{EQ}} = \frac{C_1 C_2}{C_1 + C_2} \quad (19) \qquad i_c = 2\,\frac{d}{dt}(C_{\mathrm{EQ}} V_{\mathrm{BIAS}}) \quad (20)$$

Thus:

$$V_{\mathrm{AUX}} = \int \frac{1}{C_2} i_c\,dt = 2\frac{C_{\mathrm{EQ}}}{C_2}V_{\mathrm{BIAS}} \quad (21) \qquad V_x = V_{\mathrm{AUX}} - V_{\mathrm{BIAS}} = \frac{x_{\mathrm{A}}}{g}V_{\mathrm{BIAS}} \quad (22)$$

In order to evaluate V_{OUT} the assumption of rotor at rest (i.e. no current flowing in the OPAMP) has to be removed. Indeed, V_{OUT} is used to create an electrostatic force on the armatures in order to feed the solenoid valve. The current flowing in the OPAMP is given by Eq. 23, while Eq. 24 takes into account the charges that are leaving C_2 and that are not accumulated in C_1.

$$i_F = \frac{d(CV_{\mathrm{BIAS}})}{dt} \quad (23) \qquad C = C_2 - C_1 \quad (24)$$

Therefore i_F can be evaluated in two different ways; the first (Eq. 25) considers Eqs. 23 and 24, while the second (Eq. 26) is the characteristic equation of a conductor.

$$i_F = -2\epsilon A \frac{g^2 + {x_A}^2}{(g^2 - {x_A}^2)^2} v_A V_{BIAS} \quad (25) \qquad i_F = -C_F \dot{V}_{OUT} \quad (26)$$

Hereafter, the balance of relative forces related to the rotor dynamics is considered (Eq. 27).

$$m\ddot{x}_A = -F_{EXT} + F_{EL1} - F_{EL2} \quad (27) \qquad V_C = K_{PA} V_{OUT} + K_{DA} \dot{V}_{OUT} \quad (28)$$

where F_{EXT} are the external forces acting on the GOCE, and F_{EL1} and F_{EL2} are the electrostatic forces generated between the armatures and the rotor.

$$F_{EXT} = \frac{m}{M}(T - D) \quad (29) \qquad \begin{cases} F_{EL1} = \frac{1}{2}\epsilon A_a \left(\frac{\Delta V_1}{g - x_A}\right)^2 & (30) \\ F_{EL2} = \frac{1}{2}\epsilon A_a \left(\frac{\Delta V_2}{g + x_A}\right)^2 & (31) \end{cases} \qquad \begin{cases} \Delta V_1 = V_{BIAS} - V_C - \frac{1}{2}V_x & (32) \\ \Delta V_2 = V_{BIAS} + V_C + \frac{1}{2}V_x & (33) \end{cases}$$

where V_C is the result of the PD controller over V_{OUT}, as reported in Eq. 28. Therefore, the ODEs related to the accelerometer are the ones of Eqs. 34, 35, 36 and 37. Instead, the ODEs of the flow control valve are Eqs. 38 and 39.
The orifice has been modelled considering Eqs. 40, 41 and 42, while the equation of motion of the valve is described in Eq. 43.

$$\begin{cases} \dot{x}_A = v_A & (34) \\ \dot{v}_A = -\frac{1}{m}(F_{EXT} - F_{EL1} + F_{EL2}) & (35) \\ \dot{V}_{OUT} = 2\, v_A\, V_{BIAS}\, \epsilon\, \frac{A_a}{C_f} \frac{g^2 + {x_A}^2}{(g^2 - {x_A}^2)^2} & (36) \\ \dot{I} = K_{PV}\dot{V}_{OUT} + K_{IV} V_{OUT} & (37) \end{cases} \qquad \begin{cases} \dot{x}_V = v_V & (38) \\ \dot{v}_V = \frac{1}{m_{FCV}}\left[K_{FCV}(x_0 - x_V) - c v_V - K_I I\right] & (39) \end{cases}$$

$$z = 1 - \frac{x_V}{2r_0} \quad (40) \qquad \alpha = 2\arccos(1 - 2z) \quad (41)$$

$$A_d = \frac{r_0^2}{2}(\alpha - \sin\alpha) \quad (42) \qquad m_{FCV}\ddot{x}_V = K_{FCV}(x_0 - x_V) - C v_V - K_I I \quad (43)$$

where x_0 is the rest position of the spring, defined as the diameter of the valve itself.
In order to evaluate the thrust, the mass flow rate of Xenon is evaluated in chocked condition (Eq. 46), while the force balance (Eq. 44) acting on the ions of the Xenon is integrated to find the correspondent velocity (Eq. 45).

$$e\,E = m_i \frac{dv}{dt} \quad (44) \qquad v = \sqrt{\frac{2\,e}{m_i}\Delta V} \quad (45)$$

Thus, the resulting thrust is:

$$\dot{m} = P_2 A_d \sqrt{\frac{k}{R_m T_2}} \left(\frac{2}{k+1}\right)^{\frac{k+1}{2(k-1)}} \quad (46) \qquad T = \dot{m} v = \dot{m}\sqrt{\frac{2e\Delta V}{m_i}} \quad (47)$$

Once the twelve ODEs have been found, the system has been linearised around the initial condition, through the computation of the Jacobian matrix of the system itself. Indeed, this procedure allows the evaluation of the eigenvalues, reported hereafter in Tab. 1.
The eigenvalues show that the analysed system is stiff and unstable and that these characteristics are in particular linked to the orbital part; indeed the eigenvalues with positive real part as well as the ones which are the furthest from the y-axis are all related to the orbital states.

4 Numerical integration

As already stated in section 3, there are differences of some orders of magnitude between the eigenvalues of the system; indeed to analyse it the MATLAB solver should be chosen among the

Table 1: System's eigenvalues

$\mathrm{Re}\{\lambda\}$	$\mathrm{Im}\{\lambda\}$	$\mathrm{Re}\{\lambda\}$	$\mathrm{Im}\{\lambda\}$
0.00	0.00	0.00	0.00
-75.00	171.39	-75.00	-171.39
$7.74 \cdot 10^{-8}$	$3.91 \cdot 10^{-4}$	$7.74 \cdot 10^{-8}$	$-3.91 \cdot 10^{-4}$
0.00	0.00	0.00	0.00
0.00	0.00	0.00	0.00
0.00	0.00	0.00	0.00

stiff ones, such as `ode15s, ode23s, ode23t` and `ode23tb`.
The differential system has been integrated using all of them (considering a time span of 24 hours) in order to compare the results (shown in Tab. 2). The `ode15s` is the integration scheme which exhibited the best performance in terms of numerical efficiency, considering the same tolerance among all the solvers. Hence, it was employed throughout the whole project. The stepsize of the integration is fixed step by step by the solver itself such that is possible

Table 2: Solvers comparison⋆

	ode15s	**ode23t**	**ode23tb**
successful steps	47952	$3.708 \cdot 10^6$	$2.979 \cdot 10^6$
function evaluations	97436	$3.709 \cdot 10^6$	$7.903 \cdot 10^6$
time [s]	11.7	636.3	1312.3
absolute tolerance	10^{-14}	10^{-14}	10^{-14}
relative tolerance	10^{-13}	10^{-13}	10^{-13}

⋆ `ode23s` has been discharged since it requires a longer time with respect to the other solvers to maintain the same accuracy.

to achieve an higher accuracy that a fixed step integration cannot grant. Furthermore it has been checked that it remains in such orders of magnitude for which the stability nature of the continuous-time system is preserved.
Indeed, as shown in Tab. 1, a problem that might arise is linked to the eigenvalues with positive real part, if the stepsize is high enough to make them change their original stability nature. However, as shown in Fig. 3b the stepsize never exceeds the order of 10^1 and since the positive real parts are really low (order of 10^{-8}), the integrator itself can choose the steps nonetheless. Fig. 3a shows the eigenvalues of the system, that have been plotted over the stability regions of the chosen solver, i.e. the backward differentiation formula; here, the stable region is outside the plotted curves of the BDFs, which use can be exploited writing `'BDF', 'on'` in the options of the solver.

5 The simulation framework

In Fig. 4 the procedure followed throughout the numerical simulation is showed with the aid of a flow chart:

6 System response

To appreciate the accuracy of the drag-free control, the difference between the thrust and the drag, i.e. the parameter of merit, has been plotted over six periods of GOCE orbit (Fig. 5a). Fig. 5c shows that the system response in nominal conditions is slow (thrust finds a periodicity

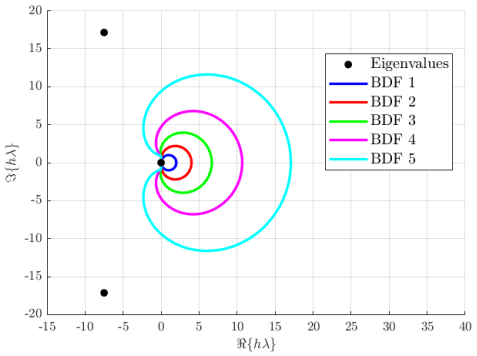

(a) BDF and eigenvalues

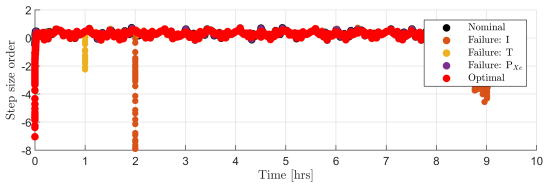

(b) stepsize

Figure 3: BFD (orders 1 to 5) stability regions with a fixed stepsize of 0.1 only for drawing purposes (Fig. 3a) and the order of the stepsize used in the integration with respect to time (Fig. 3b).

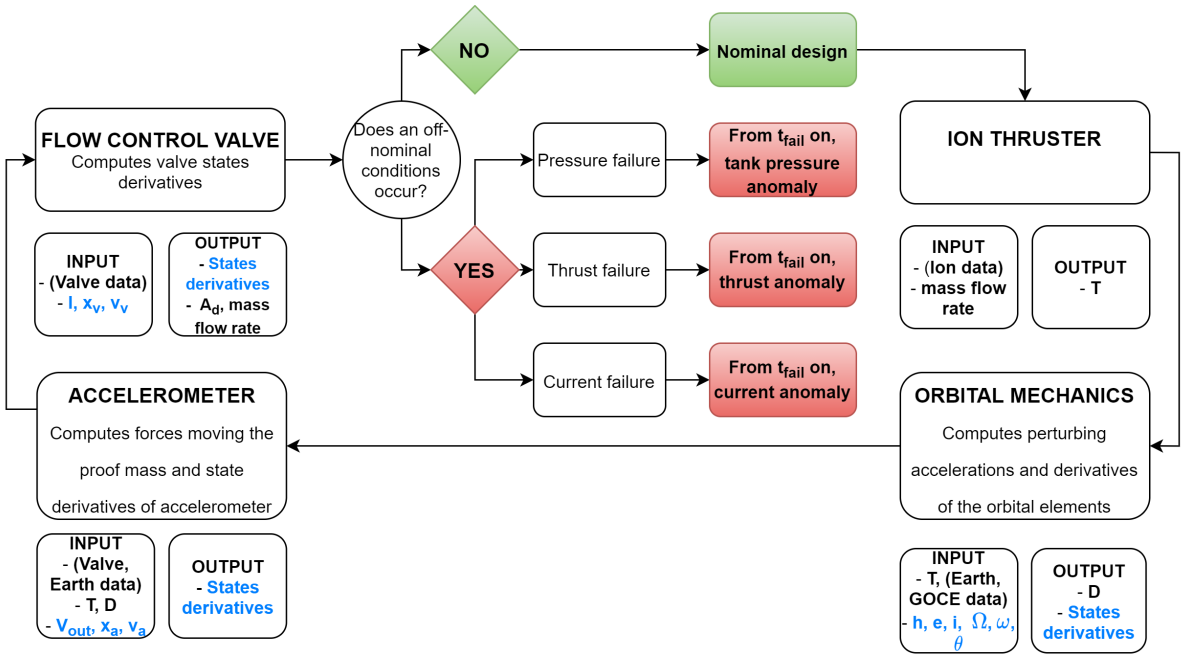

Figure 4: Simulation framework. It shows the data flow and decisions taken by the algorithm during each iteration.

after some orbits) and the drag is not counteracted efficiently.
In Figs. 5a and 5b the comparison between the nominal response and three failure modes is shown, where the latter are:

1. burn out of the coil (failure on current): the current drops to zero in a short transient, which brings the valve back to the initial position, and the thrust to 0;

2. erosion of acceleration grids (failure on thrust): the thrust decreases exponentially; this leads to an increase of the mass flow rate by opening the valve more, in order to have the thrust required to counteract drag;

3. pressurization system malfunction (failure on pressure): linear pressure drop inside the Xenon tank.

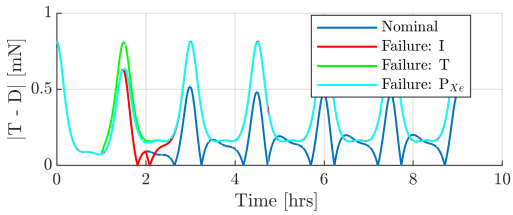

(a) difference between thrust and drag

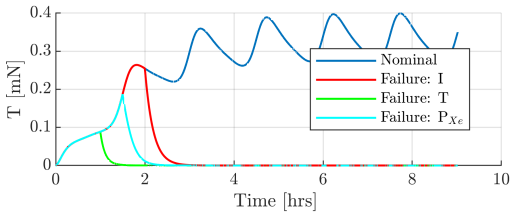

(b) thrust

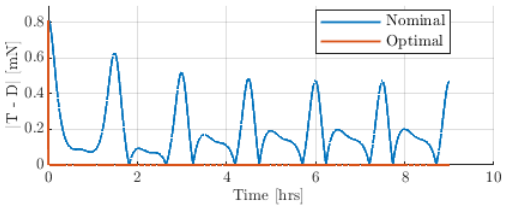

(c) difference between thrust and drag

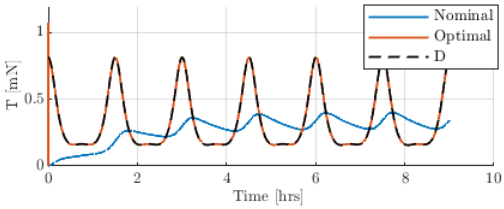

(d) thrust

Figure 5: System response in off-nominal (i.e. with failures) (Figs. 5a and 5b) and optimal conditions (Figs. 5c and 5d) with respect to the nominal ones: on the x axis the time, in seconds and on the y axis (T - D) in Figs. 5a and 5c and T in Figs. 5b and 5d, in millinewtons

A sensitivity analysis is then performed, in order to see how the system responds to a variation of the six optimisable parameters, one at a time.
Each of them is sampled 10 times, assuming values that go from the 10% to the 200% of their nominal values; then for each sample the system has been integrated with this new value, while maintaining the other parameters at their nominal ones. To retrieve the performances Eq. 48 has been employed, where `diff` is the objective function of the optimisation, in order to consider the entire analysed time window.
From Fig. 6a to Fig. 6f, sensitivity analysis results are shown for every parameter variation.

$$\texttt{diff} = \sum_{i=1}^{N_{\text{TIME STEPS}}} \mid T - D \mid_i \tag{48}$$

As K_{PA} increases, the objective function `diff` increases as well, vice versa for K_{I} and K_{IV}; whereas K_{DA}, m_{FCV}, and K_{PV} not only depict a random effect, but they do not influence the objective function significantly.

7 System optimization

Following the reasoning of the sensitivity analysis, the optimisation, which objective function is shown in Eq. 48, has been performed only over K_{PA}, K_{I} and K_{IV}. Instead, the other parameters have been maintained at their nominal values.
To perform the optimisation, the lower (`LB`) and upper (`UB`) bounds have been set for the three parameters; indeed, thanks to the sensitivity analysis, zero is considered as K_{PA} `LB` and analogously $+\infty$ as K_{I} and K_{IV} `UB`.
Instead, the values of K_{PA} `UB` and K_{I} and K_{IV} `LB` (see Tab. 3) have been set in the surroundings of their minimum ones.
As shown Fig. 5c and Fig. 5d, the accuracy of the system response with the optimised parameters is better than the one with the initial values: the thrust follows the drag profile almost perfectly.

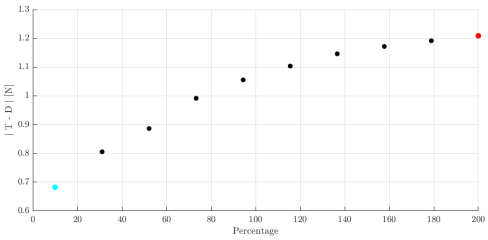

(a) Proportional coefficient of PD controller: K_{PA}

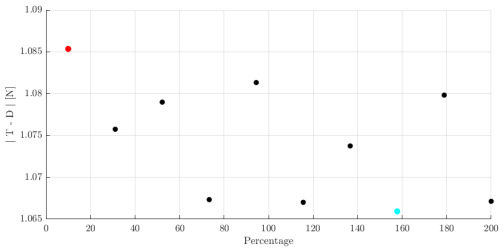

(b) Derivative coefficient of PD controller: K_{DA}

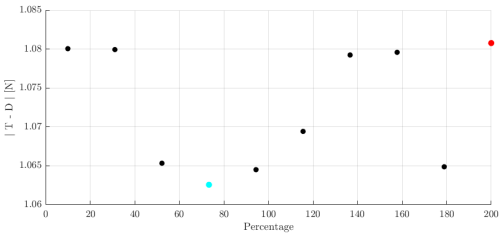

(c) Spool mass: m_{FCV}

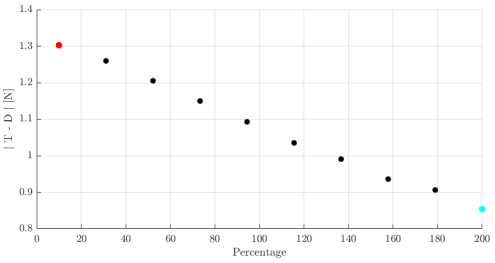

(d) Proportional current coefficient: K_{I}

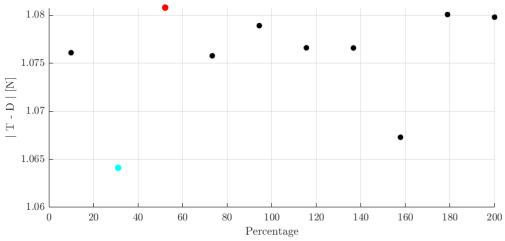

(e) Proportional coefficient of PI controller: K_{PV}

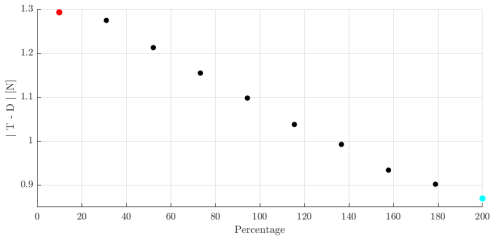

(f) Integral coefficient of PI controller: K_{IV}

Figure 6: System sensitivity analysis: on the y-axis the value of `diff` in Newtons, on the x-axis the percentage (with respect to the nominal value) considered for the particular parameter that is being analysed.

Table 3: Optimised parameters

	Nominal	**Optimised**
K_{PA} [-]	10^6	$1.422603 \cdot 10^5$
K_{I} [$\frac{N}{A}$]	0.2	$4.079903 \cdot 10^{-1}$
K_{IV} [$\frac{1}{H}$]	3	6.579797

8 Bibliography

References

[1] *Advanced Thermosphere Modelling for Orbit Prediction (ATMOP).* URL: http://www.atmop.eu/.

[2] European Space Agency. *GOCE completes its mission.* URL: http://www.esa.int/Applications/Observing_the_Earth/GOCE/GOCE_completes_its_mission.

[3] European Space Agency. *Goce Mission.* URL: https://earth.esa.int/eogateway/missions/goce.

[4] Howard D. Curtis. *Orbital Mechanics for Engineering Students.* John Wiley & Sons, 2014.

[5] Oscar Biblarz George P. Sutton. *Rocket Propulsion Elements.* John Wiley & Sons, 2017.

[6] Daniel Lamarre Damien Maeusli Michael Fehringer Gerard Andre. "GOCE and its Gravity Measurement Systems". In: (2008).

[7] C. Saunders N. Wallace P. Jameson. "The GOCE Ion Propulsion Assembly Lessons Learnt from the First 22 Months of Flight Operations". In: (2011).

[8] Bruinsma S. "The DTM-2013 thermosphere model". In: (2015).

Weights ↓	Fail (<18)	Poor (18-21)	Fair (22-25)	Good (26-28)	Excellent (29-30)
Report (50%)	• Major modelling errors (wrong assumptions, missing domains) • Simulation contains several wrong concepts • Report awfully written	• Some modelling errors (assumptions not complete, missing domains) • Simulation part contains several conceptual mistakes • English is poor	• Fair modelling (good assumptions, physics caught) • Simulation not appropriate (wrong integration scheme) • Report not clear, minor issue (typos)	• Detailed modelling (assumptions detailed and justified, all physics considered) • Minor problems with simulation (numerical issues) • Good English	• Accurate modelling (all physics considered, second order effects quantified/modeled) • Good simulation techniques (integrator, numerical issues) • Good English
Code (30%)	• Code does not run • Major algorithmic errors • Code not complete	• Minor algorithmic errors • Code is not documented • Code takes unnecessary long to run (inefficient)	• Code runs smoothly, fairly documented • Computational efficiency improvable	• Code runs smoothly, well documented • Care is taken to computational efficiency • Add-ons are produced	• Code runs smoothly, well documented • Care is taken to computational efficiency • Valuable add-ons are produced
Presentation (20%)	• Major errors in the presentation • Questions are not answered	• Poor presentation • Poor time management • Poor answers to questions	• Fair presentation • Poor time management • Weak answers to questions	• Good presentation • Good management of time • Answers not exhaustive	• Excellent presentation • Excellent time management • Satisfactory answers given

Figure 7: Rubric used for grading.